Impact of internal tides on distributions and variability of Chlorophyll-a and Nutrients in the Indonesian Seas

T. A. Capuano[1], D. Nugroho[2], A. Koch-Larrouy[1], I. Dadou[1], E. Zaron[3], K. Tran[4], V. Vantrepotte[4] and D. Allain[1]

[1]LEGOS, France, [2]ANRI, Indonesia, [3]OSU, USA, [4]LOG, France.

Corresponding author: Tonia Astrid Capuano (toniacapuano@yahoo.it)

Key Points:

- Internal tides mixing
- Chlorophyll and nutrients variability
- Spring/neap tidal cycle

Abstract

Internal tides (ITs) in the Indonesian seas were largely investigated and hotspots of intensified mixing identified in the straits in regional models and observations. Both of them indicate strong mixing up to 10^{-4}cm/s even close to the surface and show that tides at spring-neap cycle cool by 0.2°C the surface water at ITs' generation sites.These findings supported the idea of strong and surfaced mixing capable of providing cold and nutrient-rich water favorable for the whole ecosystem. However, it has never been assessed through an ad-hoc study.

Our aim is to provide a quantification of ITs impact on chlorophyll-a through a coupled model, whose physical part was validated against the INDOMIX data in precedent studies and the biogeochemical part is compared to in-situ samples and satellite products. In particular, explicit tides' inclusion within the model improves the representation of chlorophyll and of the analyzed nutrients.

Results from harmonic analysis of chlorophyll-a demonstrate that tidal forcing modify spring/neap tides' variability on the regions of maximum concentration in correspondence to ITs' génération areas and to plateau sites where barotropic tides produce large friction reaching the surface. The adoption of measured vertical diffusivities explains the biogéochemical tracers' transformation within the Halmahera Sea and used to estimate the nutrients' turbulent flux, with an associated increase in new production of ~25% of the total and a growth in mean chlorophyll of ~30%. Hence, we confirm the key role of ITs in shaping vertical distribution and variability of chlorophyll as well as nutrients in the maritime continent.

Plain Language Summary

Internal tides in the Indonesian seas have been largely studied in the last two decades and hot spots of vertical mixing have been identified in the straits along the Indonesian Throughflow. Previous model findings and satellite observations show that this mixing causes a cooling effect on the sea surface temperature in the spring-neap cycle. The effects of tidal mixing on chlorophyll has been always suspected but never clearly investigated. The aim of our study is to quantify the impact of internal tides on it through the analysis of coupled physical and biogeochemical numerical simulations. Comparisons to both in-situ observations and ocean-color satellite data are used to validate the model and demonstrate that internal tides are a key process for the vertical distribution and variability in chlorophyll as well as nutrients in the Indonesian seas.

1 Introduction

In the last two decades the Indonesian seas, with its estimated 17000 islands, have been widely investigated for its key circulation for the climate. They form the only low latitude passage between two major oceans, the Pacific and the Indian. They encompass some of the warmest surface temperatures of the world ocean that drive intense atmospheric convection [Clement et al., 2005] and are therefore able to influence climate on the global scale via atmospheric teleconnections [Neale and Slingo, 2003]. Its oceanic pathway in the Pacific to the Indian interocean exchange, which is known as Indonesian Throughflow (ITF), transports 10–20 Sv of warm and fresh waters; When not encompassing tidal forcing, models produce large biais in the thermocline and fail to correctly depict this transport [Murray and Arief, 1988; Fieux et al., 1994; Meyers, 1996; Gordon and Fine, 1996; Hautala et al., 2001; Molcard et al., 2001; Susanto and Gordon, 2005; Sprintall et al., 2009]. The Indonesian Archipelago (IA)'s bathymetry is very complex, with numerous narrow straits, shallow submarine mounts and semi-enclosed basins with sharp shelf break down to 4000m depth (Sulawesi, Molucca and Seram Seas). IA is the only region of the world where strong internal tides remain trapped in the semi enclosed seas, so that a large amount of tidal energy remains available for vertical mixing [Koch-Larrouy et al., 2007; 2008]. As a result, the salinity maximum of the North and the South Pacific Subtropical Water (NPSW and SPSW) is strongly eroded to produce a nearly homohaline water when exiting the IA [Gordon and Fine, 1996; Hautala et al., 2001; Ffield and Gordon, 1992; Gordon, 2005; Sprintall et al. 2014]. The tropical Indian Ocean thermocline is cooled and freshened by the ITF

[Song and Gordon, 2004; Gordon, 2005], creating the cool and fresh tongue induced by the ITF in the Indian ocean [Koch-Larrouy et al., 2007; Nagai et Hibiya, 2015; Nagai et al., 2017]. In fact, an averaged vertical diffusivity 10 times higher than in the open ocean (1.10−4m2/s) is necessary to reproduce the water masses as observed [Ffield and Gordon, 1992]. Actually, the mixing is non-heterogeneous [Koch-Larrouy et al., 2007; Fieldand Gordon, 1996] and higher values reaching 1.10−2m²/s can be observed above straits as shown in the INDOMIX cruise [Koch-Larrouy et al., 2015].

However, this strong mixing is not only located in the thermocline but also close to the surface. The INDOMIX cruise [Koch-Larrouy et al., 2015] revealed direct estimates of such surface intensified mixing, which had been previously detected by Alford et al. [1999] in the Banda Sea and more recently by Nagai et al. [2021] in an extensive campaign throughout the IA. All these observations suggest that internal tides' mixing at the base of the mixed layer brings cold waters at the surface, which have been proven to be critical for the climate system [Koch-Larrouy et al. 2010]. This cooling is 0.2 up to 0.8°C [Koch-Larrouy et al. 2007; 2010; Nugroho et al., 2018] and it increases the ocean heat uptake by ~20 W m^2 while it reduces the locally-driven deep atmospheric convection and the associated rain activity by as much as 20% [Koch-Larrouy et al., 2010; Sprintall et al. 2014; 2019]. This in turn regulates the amplitude and variability of ENSO, the IOD and the MJO, and thus the whole tropical climate turns out to be affected by this mixing. In fact, this cooling experiences a seasonal cycle due to monsoonal winds, with the rainy season centered on December- February (DJF), and the dry season peaking in July-August [Aldrian and Susanto, 2003; Chang et al., 2005]. The simulated and observed cooling is stronger in austral winter when the thermocline is shallower [Nugroho et al., 2018; Kida and Wijffels, 2012]. Indeed, according to Nugroho et al. [2018], the vertical mixing induced by the tides during austral winter is more efficient because the strong monsoonal winds upwell the thermocline: colder waters are closer to the surface and thus mixing imprints a greatest cooling on the surface. This spatially large cooling of the SST found during the southeast monsoon suggests that tidal mixing is likely capable of affecting the atmosphere during the season of deep atmospheric convection over the Indonesian Seas. Also at spring/neap tidal cycle a signature on sea surface temperature is observed by satellite [Ray and Susanto, 2016] and reproduced by the model including tides [Nugroho et al,. 2018]. In the face of so much evidence that mixing plays a key role in the mean state and the variability of surface flux, the question we

raise in this paper is the effects of internal tidal mixing on chlorophyll. Indeed, satellite observations have suggested that the spring-neap tide results in fluctuations of chlorophyll-a concentrations with a fortnightly period in coastal shelf waters, experiencing a seasonality due to the seasonal variation in the tidal current differences [Xing et al, 2021]. And Shi et al. [2011] were among the first in demonstrating that spring-neap tidal variation is one of the important ocean processes driving both the synoptic-scale and mesoscale changes of the ocean optical, biological, and biogeochemical properties in coastal areas encompassed within the Southeast Asian region.

Apart from the remarkable physical oceanography features above-described, the Indonesian seas are also a region of high productivity and biological diversity with intense primary production, comparable to the Atlantic and the Indian Oceans [Allen and Werner, 2002; Mora et al., 2003; Allen, 2007; 2008; Veron et al., 2009]. During the southeast monsoon (July to September, JAS period), a strong west-east Chl-a gradient is observed [Susanto et al., 2006; Kinkade et al., 1999]. Kinkade et al. [1999] also suggested a quasi-linear increase in Chl-a concentration with decreasing surface temperature, interpreting it as an effect of vertical mixing and upwelling of cold, nutrient-rich water to the stimulating surface primary production. Koropitan and Ikeda [2016], combining model results and satellite data in the Java Sea, managed to show that the seasonal variability of Chl-a distributions is highly influenced by the monsoon, through water exchange with adjacent seas and nutrient supply from river discharge. Indeed, phytoplankton blooming during the southeast monsoon is higher in general than during the northwest monsoon (January to March, JFM period). In contrast, the role of nutrient riverine input during the northwest monsoon (rainy season) is only limited in the region near river mouths or coastal areas [Koropitan and Ikeda , 2016].

Overall, the effects of mixing on biological activity has not been fully investigated, but it could be speculated that tidal mixing would have a significant impact on phytoplankton blooms through the upwelling to the surface of nutrient-rich water [Holloway and Denman, 1989; Souza and Pineda, 2001]. Using INDOMIX data [Koch-Larrouy et al., 2015], Atmadipoera et al. [2022] showed that vertical mixing (directly measured by the VMP) is the main process shaping the vertical distribution of temperature, salinity and oxygen measured in the Halmahera Sea. These authors suggested that very strong mixing is needed in this small sea where the residence time is

quite rapid (2 to 4 days). As such, vertical mixing could also dominate over the biogeochemical processes in explaining the transformation of the vertical distribution of nutrients from the Pacific Ocean to the Halmahera Sea. More concurrent physical and biogeochemical in-situ data are needed to corroborate this hypothesis and determine whether this occurs in other regions of the maritime continent. Despite its potential importance for the ecosystem, the impact of internal tides' mixing on the algae production and nutrients' distribution has not been explored yet. This paper constitutes the first study tackling this issue.

1.1 Study Objectives

Thus, our main objective is to quantify for the first time in the Indonesian region the impact, at annual and seasonal time scales, of internal tides on the supply of nutrients in the surface layers and production of chlorophyll, by comparing coupled simulations with and without tides with in-situ and satellite data.

To that end we use a coupled system based on the regional configuration developed in the INDESO project (Infrastructure Development of Space Oceanography; www.indeso.web.id/indeso_wp/index.php) ocean general circulation model (OGCM) NEMO (version 2.3) [Madec et al. 1998; 2008] and the biogeochemistry model PISCES (version 3.2) [Aumont et Bopp, 2006], which is almost the same configuration as in Gutknecht et al. (2016). However, these authors have used the internal tides' parameterization of Koch-Larrouy et al., [2007, 2010] accounting already for 100% of tidal energy, plus the explicit forcing of the tides. At 1/12° resolution the model forced by the tides is able to reproduce 75% of internal tides energy [Niwa and Hibiya, 2011]. Thus their configuration produces 175% of tidal energy. In our configuration we decided to avoid the use of the parametrization and to test only the inclusion of explicit tidal forcing on the biogeochemical modeling. The results compared to observations are shown in this paper, and suggest a general improvement of the nutrients and chlorophyll distributions in relation to Gutknecht et al. [2016], which was too productive. In addition, the properties of internal tides (generation values, dissipation rates and barotropic to baroclinic conversion of energy) used in this configuration, have been validated against INDOMIX data, as thoroughly described in Nugroho et al. [2018] and Atmadipoara et al. [2022]. We dubbed our regional coupled configuration 'INDO12BIO_V2'.

In the next sessions, we will first look at the impact of internal tides on nutrients and oxygen. Then we will assess this same impact on the new primary production rates. And at last on the chlorophyll annual and seasonal patterns. The model will be validated against several in-situ collections of nutrients samples, along with comparison to climatological distributions (CARS2009 and WOA2018). Finally the model will be compared to the chlorophyll measurements of MERIS and MODIS products, as well as estimates of new primary production therein derived.

2 Materials and Methods

2.1 Model and simulations

2.1.1 The coupled model

In the framework of the INDESO project, a physical–biogeochemical coupled model has been designed over the domain from 90–144°E to 20°S–25°N (Figure 1), widely encompassing the whole Indonesian EEZ, with a spatial resolution of 1/12°. The physical configuration is based on the NEMO-OPA 3.6 circulation model [Madec et al., 1998; Madec, 2008], and the main parameters' choice has been described in Tranchant et al. [2016]. As in Nugroho et al. [2018], this configuration includes explicit tidal forcing with 11 tidal constituents, which were derived from the TPX0.7 model [Egbert and Erofeeva, 2002] and used to force the open boundaries too. Following Shriver et al., [2012], the INDESO configuration encompassed geopotential tidal forcing for the four largest semidiurnal (M2, S2, N2 and K2) and diurnal (K1, O1, P1 and Q1) constituents. Similarly to Maraldi et al., [2013], two long-period tides (Mf and Mm) and one non-linear constituent (compound tides) M4 were also added. Explicit tides were resolved non-linearly in the model using the explicit free-surface assumption [Madec, 2008]. Apart from the version of the model code and the tidal forcing, the configuration is identical to the one described in Tranchant et al. [2016]. So, we refer to these authors for more details about the numerical setup, while the analysis of the internal tides' forcing used in this study has been performed by Nugroho et al. [2018].

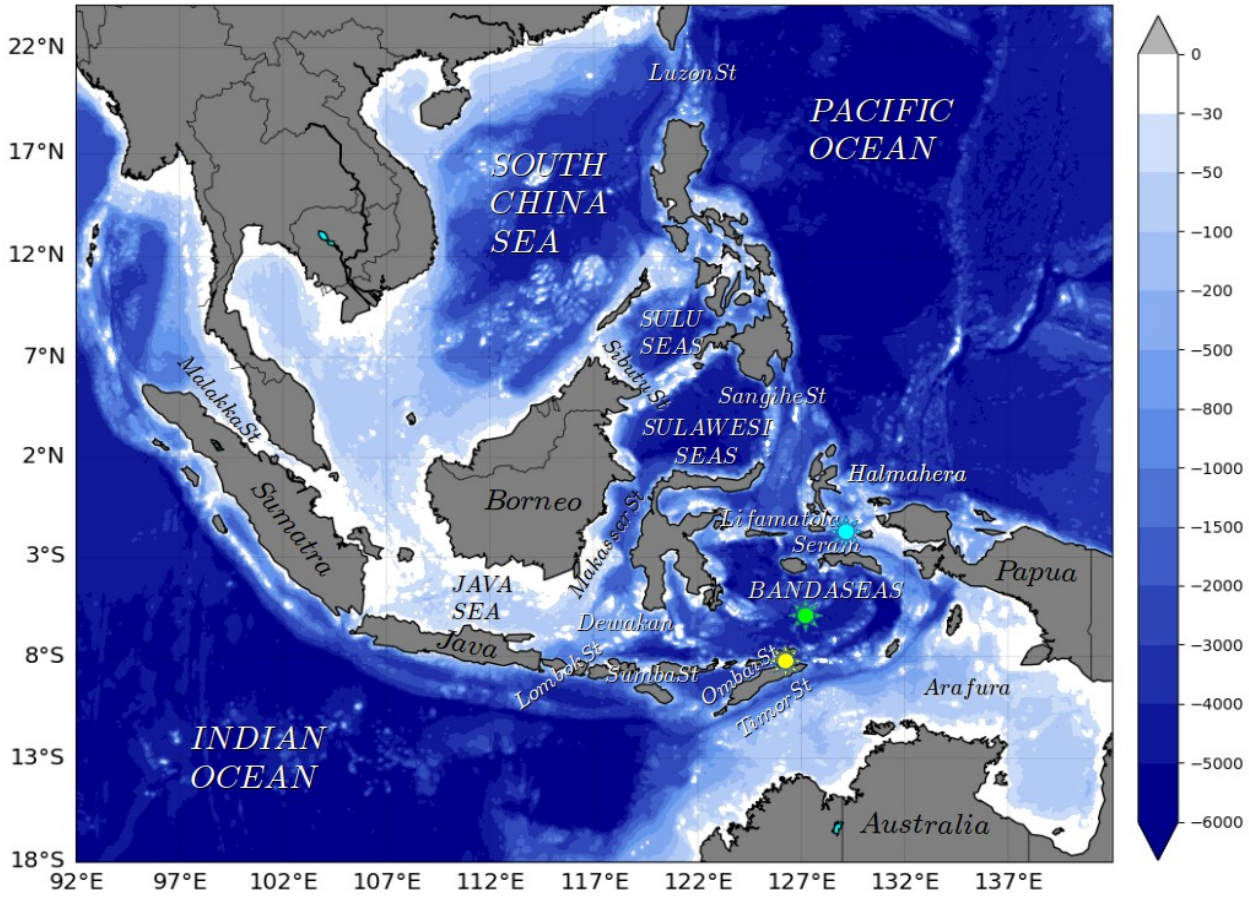

Figure 1: Bathymetry of the modeled domain, where the names of the main Indonesian seas and straits have been labeled, as well as the three INDOMIX stations used for comparison (coloured suns: cyan for Station 3, green for Station 4 and yellow for Station 5).

Dynamics of biogeochemical properties across the area are simulated by the PISCES model version 3.2 [Aumont and Bopp, 2006], and have been detailed in Gutknecht et al. [2016]. PISCES reproduces the first levels of the marine food web from nutrients up to mesozooplankton, having 24 state variables, and takes into account five limiting nutrients for phytoplankton growth (nitrate and ammonium, phosphate, dissolved silica and iron). Four living size-classified compartments are represented: two phytoplankton groups (nanophytoplankton and diatoms) prognostically predicted in carbon (C), iron (Fe), silica (Si) (the latter only for diatoms) and chlorophyll content, and two zooplankton groups (microzooplankton and mesozooplankton). Constant Carbon / Nitrogen / Phosphorus (C / N / P) Redfield ratios are supposed for all species. While internal Fe / C and Si / C ratios of phytoplankton are modeled as a function of the external availability of nutrients and thus variable, only C is prognostically modeled for zooplankton.

Biogeochemical parameters are based on the standard PISCES namelist version 3.2 [Aumont and Bopp , 2006].

PISCES is coupled to NEMO-OPA via the TOP component that manages the advection–diffusion equations of passive tracers and biogeochemical source and sink terms. In our regional configuration, called INDO12BIO_V2, physics and biogeochemistry are running simultaneously Our simulations start on 3 January 2007 from the global ocean forecasting system at 1/4◦ operated by Mercator Océan (PSY3 described in Lellouche et al. [2013]) for temperature, salinity, currents and free surface at the same date. For biogeochemistry, initial and open boundary conditions are derived from climatological data sets and, regarding the external inputs, three different sources are supplying the ocean with nutrients: atmospheric dust deposition, sediment mobilization and rivers. Please refer to Gutknecht et al. [2016] for a comprehensive description of all the biogeochemical components of the model.

2.1.2 Numerical Experiments

We run two distinct simulations:

1) the ‘CTRL’ simulation, not including any effect of the tides;

2) the ‘EXPL’ simulation, encompassing explicit tidal forcing, as explained above.

Both simulations were forced by the same buoyancy and wind forcing, and started on January 3rd 2007 until December 31st 2011. Outputs are daily average and the last four years are analyzed following a one year spin-up.

2.1.3 Harmonic Analysis

Amplitudes of the modeled and observed chlorophyll contents at the MSf tidal frequency (M2-S2, 14.8 days, spring/neap tides) was conducted through the software developed by Zaron [2018] for tidal harmonic analysis. In particular, the irregularly-sampled (gappy) time series from MODIS data were processed for each pixel using conventional least-squares harmonic analysis for the frequencies listed in Table 1: Sa (annual), Ssa (semi-annual), MSm (lunisolar monthly), MSf (lunisolar fortnightly), KOo (lunar fortnightly), and 2SM (shallow water). The least-squares resolution matrix was analyzed and in most locations the number of missing data was small

enough to permit the unambiguous identification of the harmonic constants. Experiments with seasonal modulates of the above also found significant signals; however, the accuracy of these were more sensitive to data gaps.

Darwin Symbol	Doodson number
Sa	0 565 555
Ssa	0 575 555
MSm	0 636 555
MSf	0 735 555
KOo	0 755 555
2SM	0 915 555

Table 1: Tidal frequencies used in the harmonic analysis of chlorophyll data. The frequencies are denoted with Darwin symbols and corresponding Doodson numbers following Simon [2013].

2.2 In-situ biogeochemical data : INDOMIX cruise

The INDOMIX (Indonesian Mixing program) campaign [Koch-Larrouy et al., 2015] took place in the Indonesian archipelago between the 9 and 19 of July 2010 along a transect considered one of the most energetic for internal tides' mixing and going from the Halmahera Sea to the Ombaï Strait. CTD profiles were routinely carried out, as well as measurements of nutrients, oxygen and dissipation rate at five 24h-yoyo-stations. We chose three stations for comparison with our model output: Station St3 located at the exit of the Halmahera sea, St4 in the Banda Sea and St5 at the Ombai strait (Figure 1). To co-localise the model and observations, we took the closest simulated point to the stations' coordinates; 2-day model averages were considered as measurements were performed during 2 consecutive days at the stations selected for validation.

2.3 Satellite- retrieved observations and Climatologies

2.3.1 Chlorophyll-a

Two single-mission satellite products are used for model skill evaluation, covering the whole simulated period (2007–2010). MODIS-Aqua (Moderate Resolution Imaging Spectroradiometer, EOS mission, NASA) level-3 standard mapped image product (NASA Reprocessing 2013.1). It is a product for case-1 waters, with a 9 km resolution, and is distributed by the ocean color project (http://oceancolor.gsfc.nasa.gov/cms/). The MERIS (MEdium Resolution Imaging

Spectrometer, ENVISAT, ESA) L3 product (ESA 3rd reprocessing 2011) is also considered. Its spectral characteristics allow for the use of an algorithm for case-2 waters (MERISC2R neural network algorithm; Doerffer and Schiller, 2007). It has a 4 km resolution and is distributed by ACRI-ST (http://www.acri-st.fr/). In particular, we used monthly averages for the mean state validation of our chlorophyll distribution and daily output for the harmonic analysis.

2.3.2 Nutrients and Oxygen

Modeled nutrients and oxygen distributions are validated against climatological fields of the World Ocean Atlas 2018 (WOA, 2018, 1° spatial resolution, [Garcia et al., 2018a; 2018b]), and the Commonwealth Scientific and Industrial Research Organization CSIRO Atlas of Regional Seas 2009 (CARS, 2009, 0.5° spatial resolution). Only nitrate, dissolved silica and oxygen distributions are discussed hereafter. Note that nitrate+ammonium and phosphate are linked by a Redfield ratio in PISCES.

2.3.3 Net Primary Production (NPP)

For the NPP estimate, we chose to use two production models among the three that are widely employed in the oceanic biogeochemical community. The vertically generalized production model (VGPM) [Behrenfeld and Falkowski, 1997] estimates vertically integrated NPP as a function of chlorophyll, available light and photosynthetic efficiency. It is currently considered as the standard algorithm. The alternative algorithm is an “Eppley” version of the VGPM (distinct temperature-dependent description of photosynthetic efficiencies). A complete description of the two products is available at www.science.oregonstate.edu/ocean. Due to the large uncertainty in production models, simulated NPP rates have been compared to NPP estimates derived from the two aforementioned models using MODIS ocean color data.

3 Results

3.1 The INDO12BIO_V2 validation

3.1.1 Nutrients’ Mean Patterns

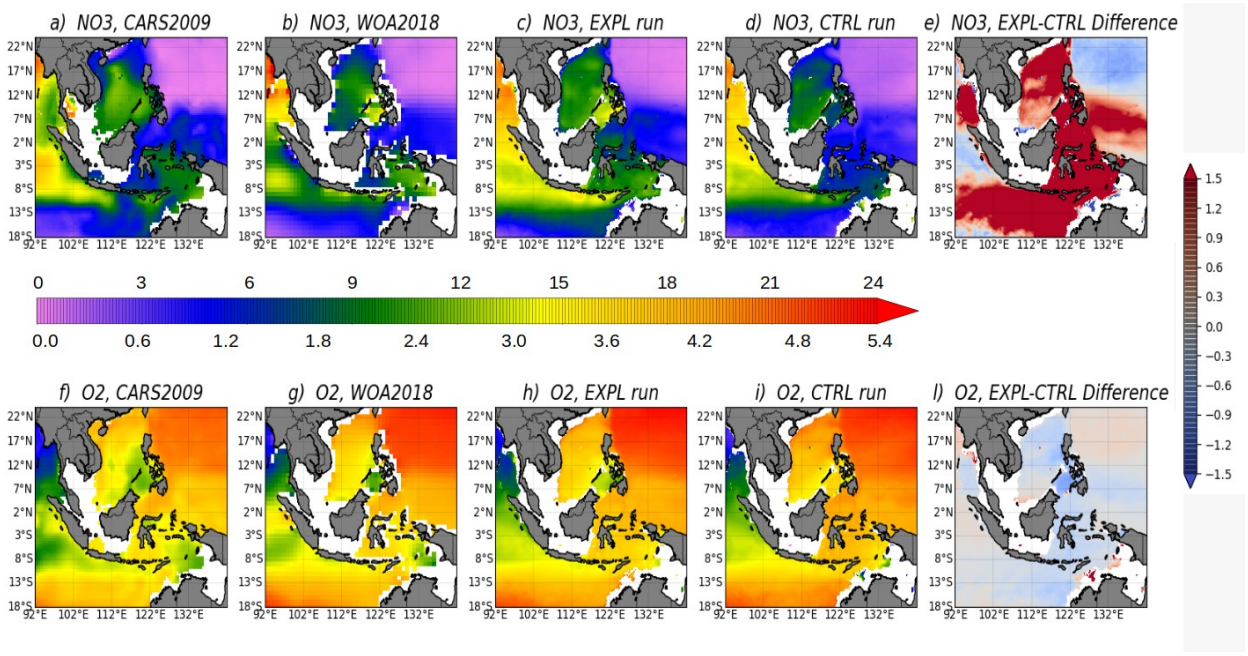

Figure 2: Annual mean of nitrate (mmol N/m³ ; upper row) and oxygen concentrations (mL O2/L; lower row) at 100 m depth from CARS (a, f) and WOA (b, g; statistical mean) annual climatologies, and from INDO12BIO_V2 as 2008-2010 averages for the EXPL run (c, h), the CTRL run (d, i) and the difference between these two simulations (e, j).

The 100m-depth annual averages (over the 2008-2010 period) of nitrate and oxygen are presented here for CARS2009, WOA2018, the two numerical configurations and their difference (Figure 2, a-j). Dissolved silica has a similar distribution to nitrate, so it is not shown. The marked meridional gradient, seen in the climatologies of the Pacific and Indian oceans, is correctly reproduced in our simulations. Nitrate maxima associated with oxygen minima are noticeable in the Bay of Bengal and Andaman Sea, reflecting discharges by major rivers (Brahmaputra, Ganges and other river systems) and the related increase in oxygen demand.

Low nitrate and high oxygen concentrations in the Sulawesi Sea reflect the signature of Pacific waters entering in the aIA, a feature reproduced in both configurations, even though in the CTRL simulation nitrate is a bit too low and oxygen is a bit too high compared to observations. The signature slowly disappears as the waters mix along their pathways across the archipelago. The resulting higher nitrate and lower oxygen levels in the Banda Sea are again retrievable only in the EXPL simulation. Higher nitrate and lower oxygen concentrations off the Sunda islands' chain in both data and model outputs reflect seasonal alongshore upwelling. The difference between the EXPL and CTRL simulations is very marked in the nitrate map (Figure 2 e) where a

strong positive bias underlines tides-related processes that enhances the 100m distribution of this nutrient, showing that EXPL is in better agreement with observations.

3.1.2 Chl-a Distribution and Seasonality

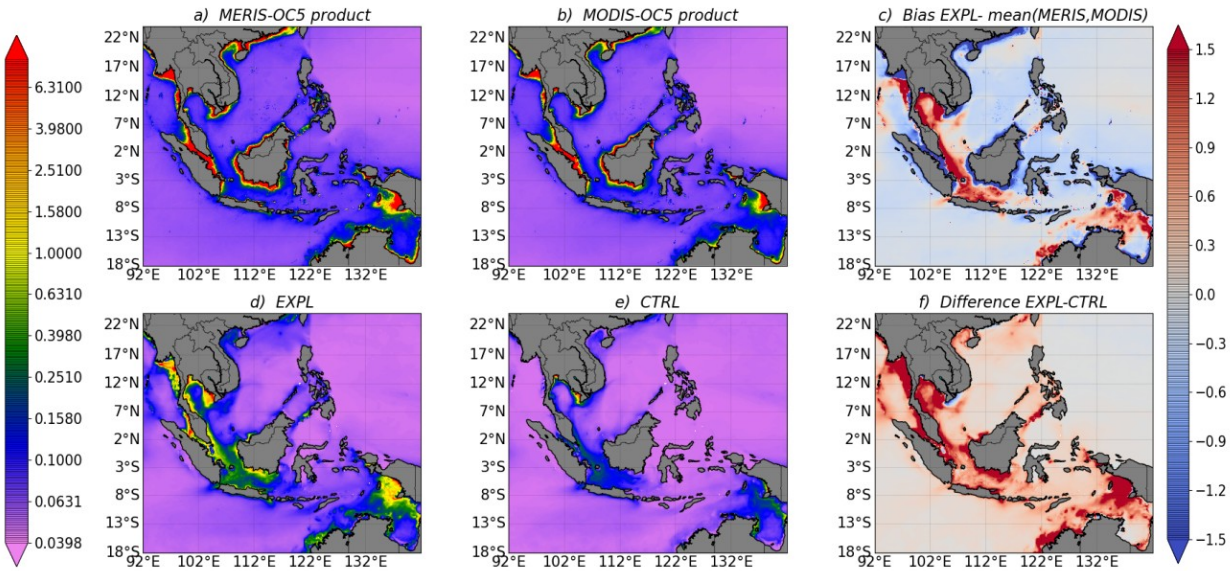

Figure 3: Annual mean of surface chlorophyll-a concentrations (mg Chl /m³) for the 2008-2010 period: MERIS case-2 product (a), MODIS case-1 product (b), the EXPL simulation (d), the CTRL run (e), the difference between the EXPL and the mean of MERIS and MODIS products and the one between the EXPL and the CTRL (f).

Our two numerical simulations reproduce the main characteristics of the large-scale distribution of Chl-a (Figure, 3, a-f) a proxy for phytoplankton biomass. In fact, both the EXPL and CTRL runs are able to capture the low Chl-a concentrations characteristic of the Pacific and Indian subtropical gyres due to gyre-scale downwelling and hence a deeper nutricline. The highest concentrations are localized along the coasts driven by rivers' nutrient supply, sedimentary processes, and upwelling of nutrient-rich deep waters. In comparison to the ocean color product of MODIS and MERIS (Figure 3, 'a' and 'b'), the EXPL configuration (Figure 3 d) performs much better, even though it overestimates the chlorophyll-a content within the Indonesian straits and underestimates it along the coasts (Figure 3 c). Much weaker values are instead found in the general distribution of the CTRL simulation (Figure 3 e), meaning that its reproduction of Chl-a concentration deviates even more from the mean patterns observed in the satellite products. Thus

302 the bias with the EXPL run is almost everywhere positive and quite high all over the modeled
303 domain (Figure 3 f).

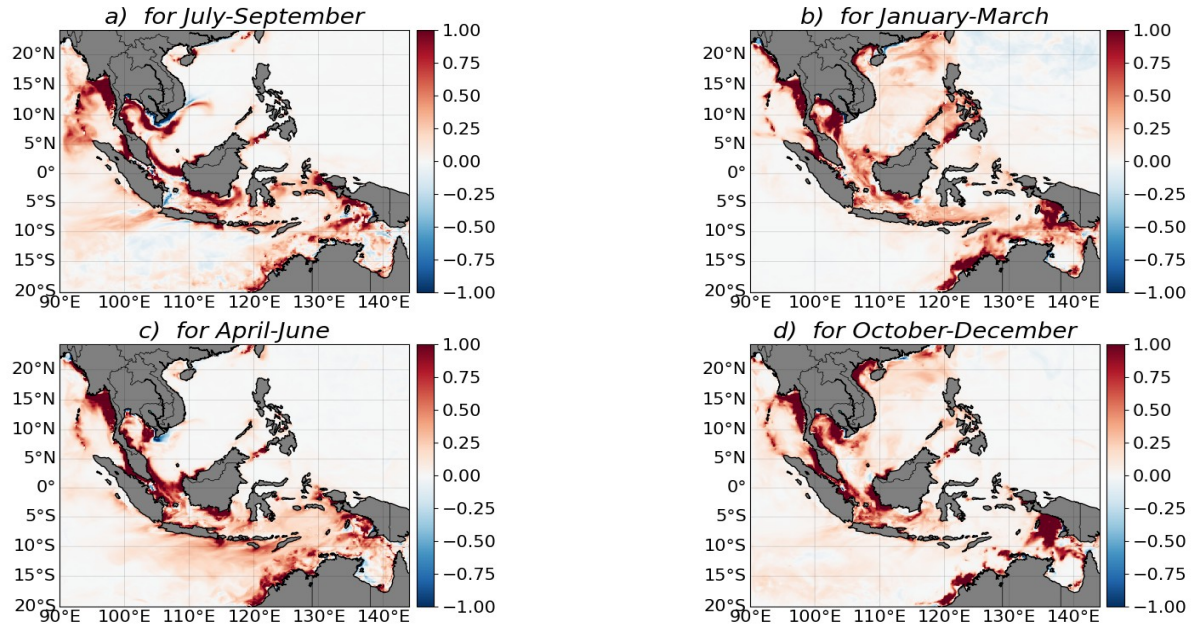

Figure 4: Chlorophyll-a seasonal anomaly for EXPL-CTRL averaged over the 2008-2010 period during the following months: (a) July–August–September, (b) January–February–March, (c) April–May–June and (d) October–November–December.

304

305 Concerning the Chl-a seasonal cycle, Figure 4 (a-d) displays the difference between the two
306 simulations by season and we observe how it is greater in the months of the SE monsoon (Figure
307 4, a and c) when the Chl-a concentration reaches its peaks. The bias between the runs is slightly
308 less marked and spread all over the domain during the NW monsoon (Figure 4, b and d), in
309 correspondence of the Chl-a minimum values. More details on the modelled Chl-a seasonality
310 will be provided in subsection b.i) where we investigated this variability in terms of amplitude of
311 the tidally- induced fortnightly modulation (MSf frequency).

312 **3.1.3 Primary Production**

313 The EXPL run reproduces the spatial distribution, as well as the mean rates of NPP over the
314 model domain (Figure 5, a-d). It is worth mentioning that NPP estimates depend on the primary
315 production model (in this case, VGPM and Eppley) and on the ocean color data used in the

316 production models. For a single ocean color product (here MODIS), NPP estimates display a
317 large variability between the two models. Hence the large uncertainty associated with these
318 products precludes a quantitative evaluation of the simulated NPP.

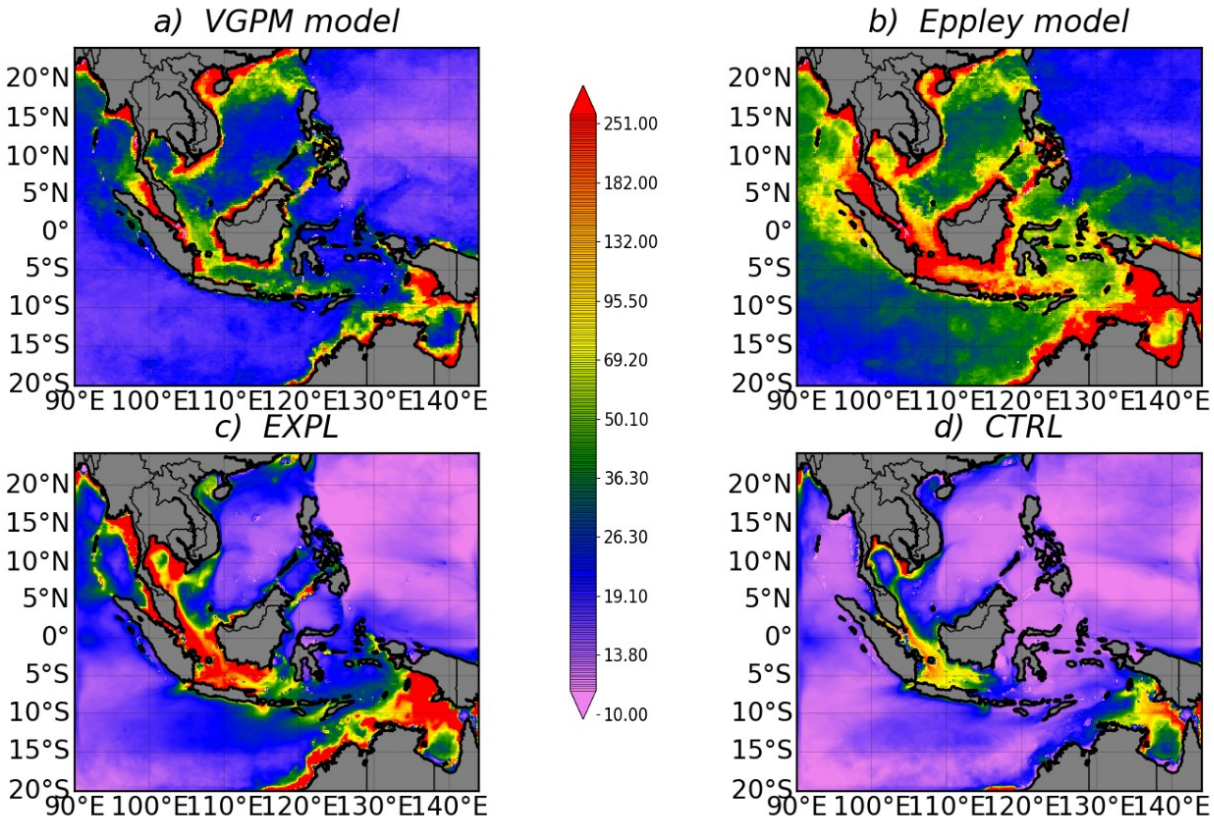

Figure 5: Annual mean of vertically integrated NPP (mmol C/m2/d) over the 3 years (2008-2010) of the analyzed simulations: VGPM (a) and Eppley (b) production models, both based on MODIS ocean color, as well as for the EXPL run (c) and the CTRL one (d).

319

320 Like for Chl-a, modeled NPP falls within the range of remote sensing derived estimates, with
321 maybe a too weak cross-shore gradient derived from the Chl-a field, especially in the CTRL
322 configuration. However, the mean NPP over the INDO12BIO_V2 domain is slightly
323 overestimated in the EXPL simulation and highly underestimated in the CTRL run.

324 **3.1.4 INDOMIX Comparison**

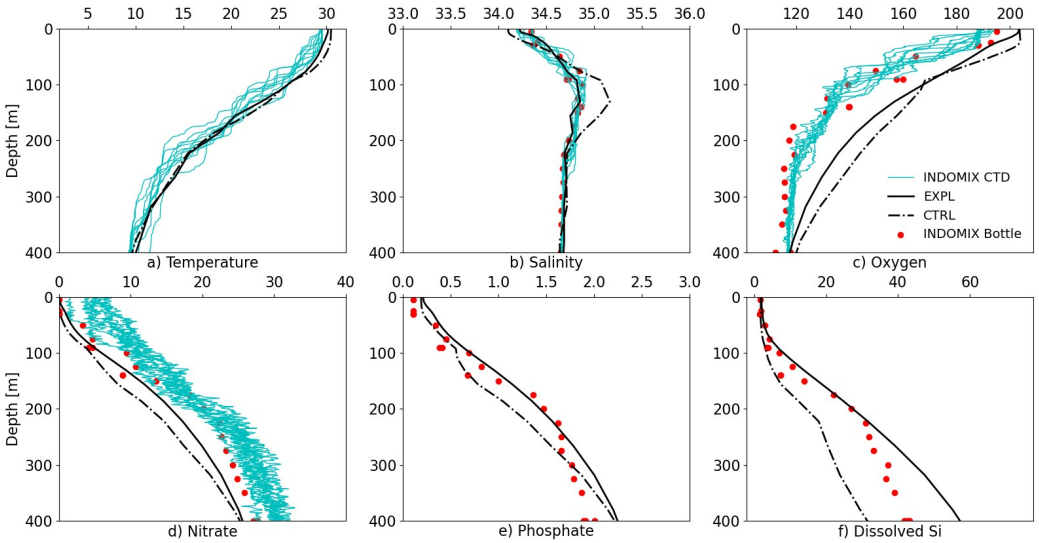

Figure 6: Vertical profiles of temperature (°C; a), salinity (psu; b), oxygen (mL O2/L; c), nitrate (mmol N/m³; d), phosphate (mmol P/m³; e) and dissolved silica (mmol Si/ m³; f) concentrations at the INDOMIX station 3 (Halmahera Sea; 13–14 July 2010). CTD (light blue lines) and bottle (red crosses) measurements represent the conditions during the cruise, 2-day model averages are shown by the black continuous line for the EXPL run and dashed for the CTRL.

Vertically, we compare our results in terms of T-S structure and biogeochemical tracers to the in-situ data collected during the INDOMIX cruise in July 2010 (Figures 6, 7 and 8). The vertical profile of temperature fairly compares with data in the Halmahera Sea (Station 3, Figure 6). Simulated surface waters are too salty and the subsurface salinity maximum is reproduced at the observed depth, albeit too high in the CTRL simulation compared to the data. Waters are more oxygenated in the model over the first 400 m, even though the EXPL curves get closer to the observational ones than the CTRL configuration. The model–data bias on temperature, salinity, oxygen and nitrate suggests that Halmahera Sea thermocline waters are not fully reproduced by the model in July 2010, since their simulated vertical profiles tend to be too smooth. Phosphate profiles better agree with observations, while dissolved silica concentrations are overestimated in the EXPL simulation below 200 m depth. It should be noted, however, that 2010 was a strong La Niña year with important modifications in zonal winds, rainfall, river discharges and ocean currents, and all these anomalies were not taken into account in the model forcings and initial/lateral conditions. Despite the bias highlighted for the Halmahera Sea station, an overall

satisfying correspondence between modeled and observed profiles is found in the Banda Sea (Station 4, Figure 7) and Ombaï Strait (Station 5, Figure 8).

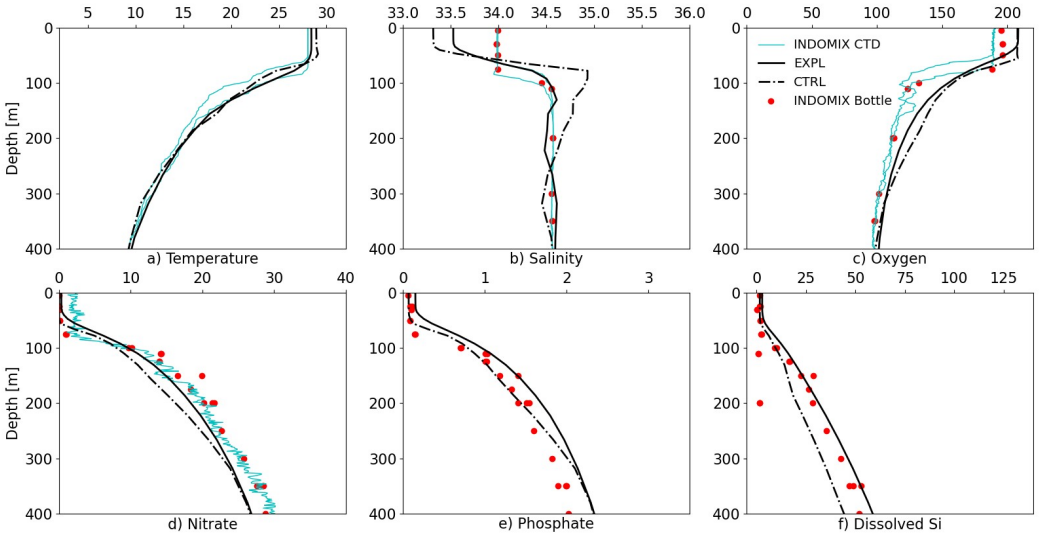

Figure 7: Same as Fig. 6 but for the INDOMIX cruise station 4 (Banda Sea; 15–16 July 2010).

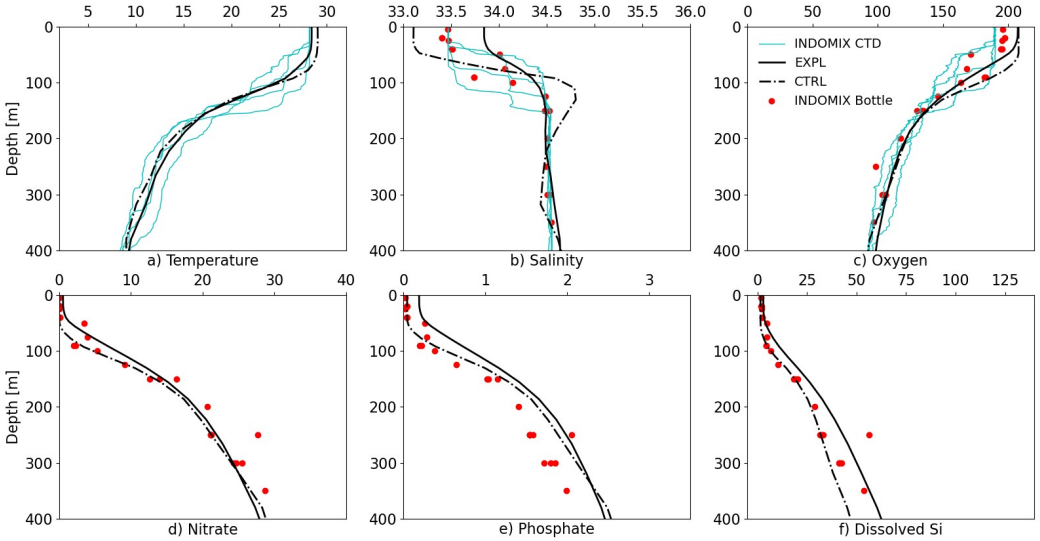

Figure 8: Same as Fig. 6 but for the INDOMIX cruise station 5 (Ombaï Strait; 16–17 July 2010).

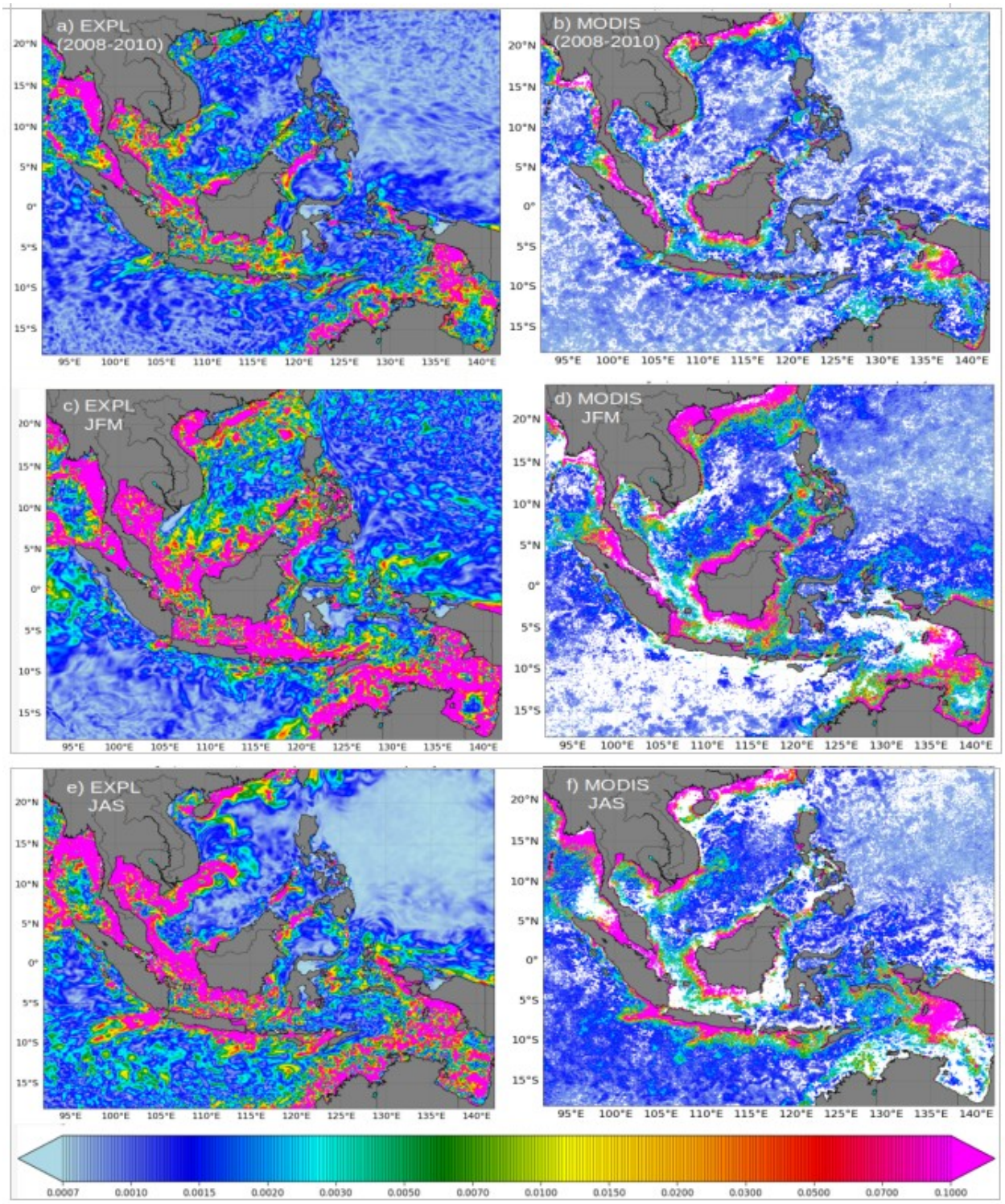

Figure 9: Amplitude of the harmonic analysis of chlorophyll-a [mg Chl/m³] at Msf frequency (M2-S2, 14.8 days, spring/neap tides) for the 2008-2010 period from the EXPL simulation (a) and based on the MODIS case-1 product (b). The lower panels show the same results but

computed for the seasons of the northwest monsoon (January to March, JFM; 'c' and 'd') and the southeast monsoon (July to September, JAS,; 'e' and 'f').

345 **3.2 The Effects of IT'S Mixing on Chl-a and Nutrients**

346 **3.2.1 MSf of CHL**

347 What our EXPL configuration is, at present, able to accurately capture is the fortnightly
348 (14.8 days, spring tides-neap tides) modulation, produced by the combination of the M2 and S2
349 semidiurnal tides, on the Chl-a variability. Over a fortnight, the Chl-a range at the MSf frequency
350 is between 0.07 and 0.1 mg Chl/m^3 in the main regions of intensified mixing due to internal tides
351 (Figure 9 a), such as Dewakang, Makassar, Ombai and Lifamatola Straits as well as in the
352 Islands chain between Sulu and Sulawesi Seas, at the entrance of the Halmahera Sea or in the
353 Sangihe Island. In Lombok and Sibutu straits, it is even larger than 0.1 mg Chl/m^3 and quite
354 strong also in the shelf-break of the Australian shelf, as well as in the northern part of the China
355 Sea. This signal is particularly enhanced along the coasts, like in the satellite-derived map from
356 the MODIS case-1 product (Figure 9 b), and during the Southeast monsoon (July to September,
357 JAS; Figure 9 c) in comparison to the Northwest monsoon estimate (January to March, JFM;
358 Figure 9 d). Our findings confirm the hypothesis of Xing et al. [2021] that spring-neap tide
359 induces fluctuations of Chl-a concentrations with a fortnightly period in Indonesian shelf waters,
360 whose seasonality was directly driven by the seasonal variation in tidal current differences.

361 These authors recognized that a large number of missing values and low observation
362 frequency in satellite-derived Chl-a are the major obstacle to investigating the regional pattern
363 showing where and to what extent the effects of spring-neap tide have on Chl-a and on its
364 seasonal variations within a relatively large region. In our case we tried to overcome this
365 problem by using the interpolation technique of Zaron [2018] for analyzing the gappy and noisy
366 data of Chl-a from MODIS. Through this methodology, we also performed the computation of
367 the least-squares standard error and masked out the values where the amplitude is smaller than
368 1.7 this error (Figure 9 b, d and f). We chose this threshold after having carried out several tests
369 and found out that for values higher than 1.7 no significant changes were visible for the areas of
370 major concern for our study, meaning the Indonesian hot spots of tidally-induced mixing. In the
371 MODIS maps of Figure 9 (b, d and f) we can observe that the amplitude for Chl-a variability at

372 the fortnightly cycle (MSf) is generally greater than the noise estimate. Relevant amplitudes exist
373 in other interesting places, for example along the NW coast of Australia, where the amplitude is
374 large and the phase is spatially continuous (not shown). Same thing between the Sulu and
375 Celebes Seas, the Coral Sea and the Gulf of Carpentaria, in the Strait of Malacca, and also
376 between Taiwan and Hong Kong. The details, of course, depend on the threshold for masking
377 areas as signal or noise. Also, these maps use spatially-smoothed data, with an averaging scale of
378 about 1/4°. Further details on the technical aspects of the 'averaging' methodology are out of the
379 scope of the present paper and constitute the topic of a companion manuscript in preparation by
380 Zaron et al. [2022]. What we reckon important to underline for the present study is the tidal
381 signature at the MSf frequency detected on the Chl-a concentration, that we were able to capture
382 both in the modeled and observed estimates and showing as well a strong seasonality in relation
383 to the Indonesian monsoonal system.

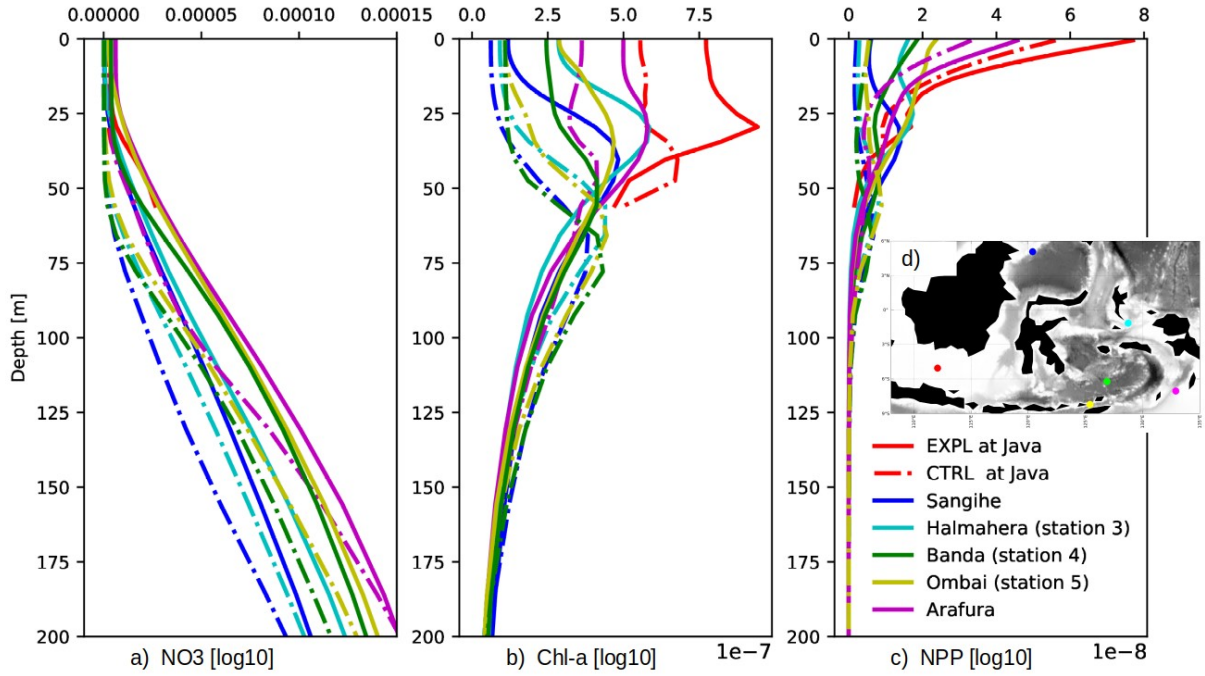

Figure 10: Vertical profiles of Nitrate (mmol N/m³; a), chlorophyll-a (mg Chl /m³; b) and NPP (mmol C/m2/d; c) at the sites where the latter had the strongest values and shown in the map of subplot 'd'. The continuous curves are for the EXPL simulation and the dashed one for the CTRL run.

384

385 **3.2.2 Biogeochemical Profiles and their Properties' Transformation**

To better assess the effects of IT's mixing on the nutrients and CHL variability at depth, we looked at profiles of Nitrate, CHL and NPP at the sites where the latter had the highest values in the modeled domain (Figure 10, a-d). We see how also in the vertical the difference between the Explicit tides curves (continuous) and the CTRL ones (dashed) is quite marked at the sites of intense internal tides' mixing signature, as at the INDOMIX Stations 3, 4 and 5 (respectively cyan, green and yellow points in the map of subplot 'd'). These differences are also particularly enhanced over the 'plateau' sites like in the Java sea in red and in the Arafura Sea in magenta. At all these sites we can observe a stronger uplift of nutrients in the EXPL configuration, where the nitrate, Chl-a and NPP peaks reach closer to the surface, confirming our hypothesis on the role of internal tides in upwelling nutrient-rich deep waters at the locations of strong mixing.

For the nutrients' profiles sampled at the INDOMIX Station 3, we also applied the one-dimensional advection/diffusion model of Ffield and Gordon [1992], thoroughly described in Atmadipoera et al. [2022] for the cruise case study. These authors used such a simple model to test the transformation of South Pacific Subtropical Water (SPSW) from the entrance to the exit of Halmahera Sea, by taking a vertical diffusivity profile from INDOMIX direct microstructure measurements and water properties measured in the Pacific side [Koch-Larrouy et al., 2015]. Here, we apply the same methodology to the biogeochemical tracers' profiles of nitrate, phosphate, silicate and oxygen to verify if also in the case of the biogeochemical tracers the tidally-induced vertical mixing represents one of the main sources of nutrients' transformation through the Halmahera Sea. Indeed, in Figure 11 we observe how the nutrients' profiles at the entrance of this sea (1st column) get partially modified through their pathway (2nd column) by applying vertical diffusion coefficient as measured at station 1 (Kz_1, Figure 16c of Atmadipoera et al. [2022]) by direct microstructure and become almost completely transformed at the exit (3rd column) after two days of residence. Two days more mixed by the vertical diffusivity measured at station 3 (Kz_3, Figure 16c of Atmadipoera et al. [2022]) produced completely mixed properties (fifth column). In fact, the nutrients' profiles calculated by the 1D mixing hypotheses (red line) show very good agreement with the mean profiles measured at sea (black thick lines for stations C1, C2 and C3). This calculation allows us to conclude that vertical mixing induced by the tides is the main mechanism responsible for the drastic change observed in the nutrients' vertical structure. This result is in good agreement with the estimates of Nagai et al. [2017] reporting that

416 76% of the ITF water masses' transformation in the Halmahera Sea is driven by internal tides'
417 diapycnal mixing.

418

419

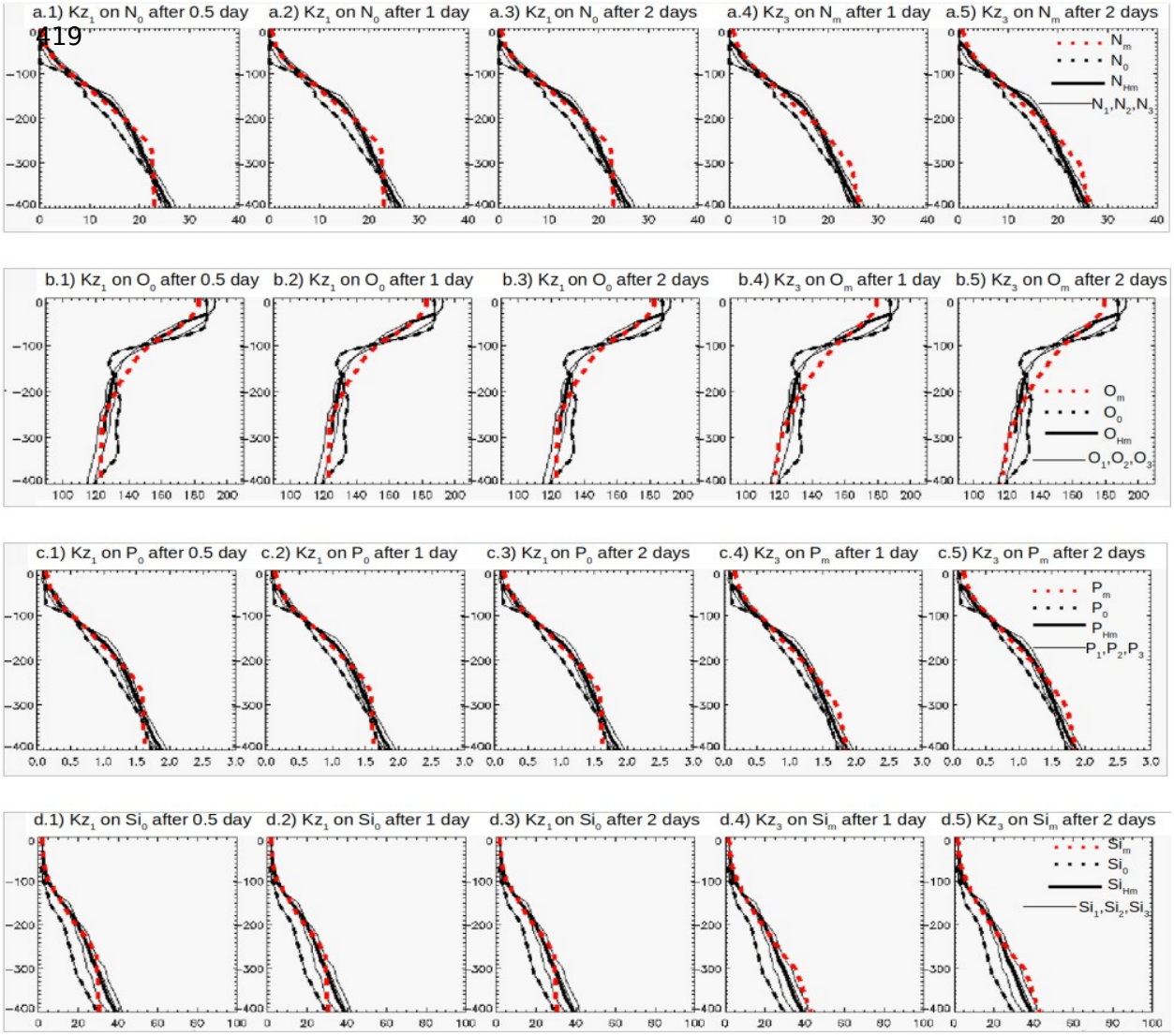

Figure 11: Vertical profiles of Nitrate (N, a 1-5), Oxygen (O, b 1-5), Phosphate (P, c 1-5) and Silicate (Si, d 1-5) and at the entrance of the Halmahera Sea (station C0, black dotted line) compared to their mean profile within this region (average of sites C1, C2, and C3, thick black line, and thin black line corresponds to each profile in C1, C2, and C3). Red dotted line is the result of the 1D diffusion model using Kz measured by VMP from INDOMIX and the C0 profile. The 1st column shows the profile obtained after 0.5 days, 2nd column after 1 day, and 3rd column after 2 days using the Kz₁ measured in C1 by the INDOMIX microstructure profile . The 4th and 5th columns correspond respectively to 1 day and 2 days after applying the Kz₃ value from station C3. We refer to Atmadipoera et al. [2022] for the Kz₁ and Kz₃ values and profiles.

3.2.3 Nutrients' Turbulent Fluxes

With the aim of quantifying the above-mentioned nutrients' uptake at the base of the euphotic layer by vertical turbulent diffusion and the associated potential new production, we follow Eppley and Peterson [1979] to calculate this nitrate supply by vertical turbulent flux (Nflux) as:

$$NFlux = Kz * dNO3/dz \quad \text{Equation 1}$$

where Kz is vertical turbulent diffusion coefficient and dNO3/dz is the nitrate vertical gradient. Here the assumption that all the nutrients are consumed by phytoplankton was adopted, while for the depth of the euphotic layer, a light attenuation coefficient for clear waters was used and considered a good approximation for the types of waters analyzed in this exercise.

Then by multiplying this turbulent flux (Nflux) by the Carbon/ Nitrogen Redfield ratio (R_C/N) and the Carbon molar mass (MC) we can obtain an estimate of the potential new production:

$$PNP\ (gC/m^2/d) = MC * R\_(C/N) * Nflux \quad \text{Equation 2}$$

From combining Equation 1 and Equation 2 we obtain values for the 3 INDOMIX Stations, used for the vertical profiles' validation, within the order of 0.1- 0.13 ($gC/m^2/d$), that compared to the total estimates issued from the model and integrated over the euphotic layer, provide a ratio in the order of ~ 25%:

$$PN\ (gC/m^2/d) = 0.1 \quad 0.11 \quad 0.13$$

$$PN/PPT\ (gC/m^2/d) = 0.26 \quad 0.21 \quad 0.24\ (x\ 100, \text{for percentage})$$

And if we want to compute the associated increase in mean Chl-a (INC_CHL), always within the euphotic layer, we can use the following equation [Geider et al., 1997; Aumont et al., 2015] :

$$INC\_CHL\ (mg\ Chl/\ m^3) = PNP * R\_(CHL / C) * \boldsymbol{\Delta\tau} \quad \text{Equation 3}$$

where 'R_ (CHL / C)' is the chlorophyll/ carbon Redfield ratio and $\boldsymbol{\Delta\tau}$ is the mean advection time in the area, for instance 2 days as sampled during the INDOMIX cruise in the Halmahera Sea (Station 3). At the three INDOMIX sites, the estimates from Equation 3 approximate the MSf values of 0.06-0.1 mg Chl/m^3, ranging from a minimum value of 0.07 for a Chl/C ratio of 0.033 to a max value of 0.12 for a ratio equal to 0.055, corresponding to a growth of about 30% of the mean value of chlorophyll concentration within the euphotic layer. The latter is a significant result considering that we are not within the extremely productive Eastern Boundary Current Systems and if we take into account the instantaneous nature of the real processes, in relation to our estimates that were averaged over the two days of the observed advection time.

4 Discussion and Conclusions

Tides are the dominant hydrodynamic processes in most continental shelf seas and have been proven to have a significant impact on both marine ecosystem dynamics and biogeochemical cycles [Shi et al., 2011; Xing et al., 2021]. In the case of the Indonesian seas, where tidal generation and dissipation assume remarkable values, among the highest within the world ocean, fluctuations at tidal frequencies are expected to be particularly marked at the sites of intense IT's mixing and to have direct effects on the surface and vertical behaviors of biogeochemical tracers.

Building upon the numerical work of Nugroho et al. [2018], we couple these authors' physical configuration with a biogeochemical model to assess the impact of the explicit tides' inclusion on the distributions and variability of nutrients and chlorophyll within the Indonesian seas (Figure 1). We show that in our INDO12BIO_V2 configuration the large-scale distribution of nutrient, oxygen, chlorophyll-a and NPP (respectively Figures 2, 3 and 5) are well reproduced in both the CTRL simulation (without tides) and the EXPL (with tides) configuration. However, their cross-shore gradients are correctly represented only in EXPL, given that the CTRL run misses the tides-driven processes vital for the coastal patterns of these biogeochemical tracers. We also verified that the vertical distribution of nutrients and oxygen is comparable to in situ-based datasets from the INDOMIX cruise (Koch-Larrouy et al., 2015; Figures 6, 7 and 8). This matching is particularly satisfying in the EXPL simulation where the inclusion of tidal forcing allows to capture the local transformation of the regional water-masses by hydrodynamics across the Indonesian archipelago. This is the reason why nutrients and oxygen profiles well agree with

observations in the Banda Sea and in Ombai Strait (respectively Stations 4 and 5 of INDOMIX), located at the exit of the archipelago, whereas a weaker correspondence is found at its eastern entrance (Halmahera Sea, Station 5). The latter is probably explainable with the lack, in the model atmospheric and oceanic forcings and in its lateral boundary conditions, of all the changes observed in 2010 due to the strong La Niña's effects. Another possible cause is the thermohaline bais found for subtropical waters in the PSY3 reanalysis [Lellouche et al., 2013] that we used to force the open boundaries of our simulations.

In terms of the CHL seasonal behavior, we show that the bias between the EXPL and the CTRL simulations, meaning the effect of including tidal forcing in the model, is strongest during the southeast monsoon months (Figure 4, a and c) and less marked in the northwest monsoonal period (Figure 4, b and d). This is probably related to the impact of internal tides' mixing has on the surface seawater properties, as Kida and Wijffels [2012] and Nugroho et al. [2018] have reported, on basin average, a stronger SST cooling induced by this mixing during the southeast monsoonal season. On the other hand, the same authors highlighted a decrease in this cooling during spring and autumn, when the monsoonal winds are weaker. We thus demonstrate that chlorophyll distribution is impacted by the same tidally-induced mechanisms of seasonality as previously seen for the SST cooling, with relevant implications for the whole marine ecosystem at seasonal and intraseasonal scales. Indeed, according to Nugroho et al. [2017], the vertical mixing induced by the tides during austral winter is more efficient because the strong monsoonal winds upwell the thermocline: colder waters are closer to the surface and thus mixing imprints a greatest cooling on the surface. This spatially large cooling of the SST found during the southeast monsoon suggests that tidal mixing is likely capable of affecting the atmosphere during the season of deep atmospheric convection over the Indonesian Seas.

Regarding the surface Chl-a variability in relation to internal tides' effects, we show that M2 and S2 semidiurnal tides combine to produce a fortnightly (14.8 days, spring tides-neap tides) modulation (Figure 9 a), that was already documented on the SST field in previous studies [Ffield and Gordon, 1992; 1996; Ray and Susanto, 2016; Nugroho et al., 2017], and on the Chl-a in a companion paper of Zaron et al. [2022]. Over a fortnight the chlorophyll-a range is between 0.06 and 0.1 in the main regions of intensified mixing induced by internal tides and this distribution well compares with the same estimate from satellite-retrieved observations (Figure 9

b) and analyzed through the Zaron [2018]'s software, able to treat gappy and noisy data as the one we used from the MODIS case-1 product (Figure 9 b, d and f). More detail on this analysis can be found in Zaron et al. [2022]. A stronger signal in the modeled and observed MSf amplitude of Chl-a was detected during the southeast monsoon (July to September, Fig. 9 e and f), in correspondence to the more enhanced cooling occurring at the surface in this season (Figure 10c of Nugroho et al. [2018]). During the northwest monsoon (January to March, Fig. 9 c and d), the signal is still strong, but the highest values are more concentrated within the regions of intensified mixing, as reported for the seawater cooling in the SST seasonal map of Nugroho et al. [2018] (Figure 10d of their paper).

The impact of IT's mixing on the biogeochemical tracers is quite marked in the vertical too, as displayed in the profiles of nitrate, chlorophyll and NPP of Figure 10 (respectively a, b and c) extracted at the sites where the latter had the greatest values (Fig. 10 d). Here, we observe an enhanced uplift of nutrients, from the deeper to the upper layers of the water column, for the simulation encompassing the explicit tidal forcing (EXPL, continuous line), well visible not only a the predictable hot spots of mixing, like the INDOMIX Stations analyzed (3, 4 and 5), but also at the sites located over the plateau. For the first ones, we followed the simple advection/ diffusion model applied by Atmadipoera et al. [2022] on T-S in order to verify if the intense turbulent mixing measured at Station 3 during INDOMIX can reproduce the nutrients' transformation from the entry point to the exit of Halmahera Sea in a couple of days (Figure 11). The observed biogeochemical tracers, as the physical ones, at the exit of Halmahera sea, can be reproduced with only the 4 days of vertical diffusivity at station 1 and 3 (2 days each) meaning that tidally -induced diapycnal mixing triggers most of the nutrients' vertical changes in the areas where internal tides are particularly energetic.

As this vertical diffusivity is so important in the region, we made an analytical calculation to quantify how much nutrient flux could reach the surface due to these Kz and to what Chl-a anomalie it would correspond. We calculate the turbulent uptake of nutrients, displayed in Figure 10 within the euphotic layer, by applying Equation 1, where we multiplied the vertical diffusion coefficient (Kz) by the nutrient gradient, in this case nitrate (NO3) since it was considered the limiting factor. We then used the product of this turbulent flux to get an estimate of potential new production (PNP, Equation 2) that compared to the total value from the model gives an order of

about 25% of positive anomaly of NPP for the Halmahera Stations. And we also calculated the associated growth in the mean Chl-a concentration (Equation 3), obtaining an estimate of about 30% increase when taking into account a mean advection time of 2 days as observed in the Halmahera Sea (Station 3). In reality, the model may underestimate such an increase in the NPP and in the mean Chl-a since with the current resolution of our EXPL configuration (1/12°) we are sub-estimating the tidal energy reservoir by ~30%. Having a higher spatial resolution or adding a 0.3 of the internal tides' parameterization of Koch-Larrouy et al., [2007, 2010] may increase this effect in the model. Despite of this limitation and in light of all the findings above-summarized, we can affirm that:

1. Our INDO12BIO_ V2 configuration is generally in good agreement with observations of chlorophyll at the surface and for the 3D distribution of nutrients;
2. The inclusion of explicit tides within the model (EXPL) improves the representation of chlorophyll-a and the other biogeochemical tracers analyzed in this study (Nitrate, Phosphate, Oxygen, Silicate) ;
3. Tidal forcing modify spring/neap tides' variability on the regions of max Chl-a, with an order of magnitude comparable to the total signal ;
4. The tidal signature on Chl-a variability follows the seasonality of its surface concentration, closely related to the one of the SST regional cooling;
5. A simple diffusion model shows that tidally- induced diapycnal mixing triggers most of the nutrients' vertical changes in the areas where internal tides are particularly energetic;
6. The potential new production associated with the nutrients' turbulent uptake is ~25% of the total and the increase in mean Chl-a is ~30%, which are significant results for this oceanic region.

This study extends the findings of Zaron et al. [2022] on the tidal low-frequency variability of chlorophyll-a to those regions of the IA known as hotspots of internal wave-driven mixing, as shown in their TPX09 diagnostics (Figure 7 of their paper), but where the harmonic analysis of the gappy satellite data hampered to retrieve a significant signal at the MSf frequency. In fact, using the output of a coupled numerical simulation, forced by explicit tides, we were able to map most of the Chl-a components phase-locked with spring/neap tidal cycle and to also depict their

561 marked seasonality. Besides, our results complete the picture of Atmadipoera et al. [2022] on the
562 vital role assumed by internal tides' mixing in transforming thermohaline properties and
563 controlling the vertical distribution of oxygen measured in the Halmahera Sea, and demonstrate
564 that nutrients' variability are also driven by such a mechanism in this Indonesian subregion. We
565 additionally suggest that for the Chl-a, these turbulent interactions are at play even at other sites
566 of enhanced mixing and, in particular, over the Java and Arafura plateaus, where barotropic tides
567 on the shelf produce intensified mixing interacting with the bottom [Nugroho, PhD; Zaron et al.
568 2022].

569 Hence, we conclude that internal tides are a dominant process within the Indonesian
570 archipelago not only for the physical processes that rely on the vertical mixing they generate, but
571 also for the local biogeochemical cycles. Indeed, relevant portions of the primary production and
572 the associated growth in mean Chl-a concentration, occurring within the euphotic layer, directly
573 depend on the turbulent uplift of nutrients entrained by internal tides along the water column.
574 Higher resolution numerical experiments, able to capture finer scales dynamics, would be
575 required to solve the whole spectra of internal tides' forcing and simulate the entire 100% energy
576 production linked to their breaking. Concomitantly, more field observations would help to
577 further investigate if the fluctuations at tidal frequencies, previously reported in the SST cooling
578 and presently recovered in the biogeochemical tracers' distributions, could also affect the
579 atmospheric components of the Indonesian climate system.

580 **Acknowledgments**

581 The author's research as postdoctoral fellow at IRD-LEGOS has been funded by the Agence
582 Française de Développement (AFD) under the framework of a Fund for Technical Expertise and
583 Experience Transfers (FEXTE), which supports technical-cooperation programs and project-
584 preparation studies.

585

586 **References**

587 Aldrian E, Susanto DR (2003) Identification of three dominant rainfall regions within
588 Indonesia and their relationship to sea surface temperature. Int J Climatol 23:1435–1452.
589 Alford, M. H., M. C. Gregg, and M. Ilyas (1999), Diapycnal mixing in the Banda Sea:
590 Results of the first microstructure measurements in the Indonesian Throughflow,
591 Geophys. Res. Lett., 26(17), 2741, doi:10.1029/1999GL002337.
592 Allen, G. R. (2007), Subtidal macrobenthic structure in the lower lima estuary, NW of
593 Iberian Peninsula, Aquat. Conserv. Mar. Freshw. Ecosyst., 44(August), 303–313,
594 doi:10.1002/aqc.
595 Allen, G. R., and T. B. Werner (2002), Coral reef fish assessment in the “coral traingle” of
596 Southeastern Asia, Environ. Biol. Fishes, 65, 209–214, doi:10.1023/A:1020093012502.
597 Allen, G. R. (2008), Conservation hotspots of biodiversity and endemism for Indo-Pacific
598 coral reef fishes, Aquat. Conserv., 18, 541–556, doi:10.1002/aqc.880.
599 Atmadipoera, A.S., Pariwono, J.I., Setiawan, A., Kusumo, S. (1999). Physical oceanography
600 of the northeastern Jakarta Bay derived from coastal monitoring buoy. Proceeding of the
601 5th International Marine Science Symposium on the physical, biological, chemical,
602 and geological processes in the Pacific and Asian Marginal Seas. Kagoshima
603 University, Japan.
604 Atmadipoera, A., Koch-Larrouy, A., Madec, G., Grelet, J., Baurand, F., Jaya, I., Dadou,
605 I. (2022). Part I: Hydrological properties within the eastern Indonesian Throughflow
606 region during the INDOMIX experiment. Deep Sea Research Part I: Oceanographic
607 Research Papers. 182, 103735, 0967-0637. https://doi.org/10.1016/j.dsr.2022.103735.
608 Aumont, O. and Bopp, L.: Globalizing results from ocean in situ iron fertilization studies,
609 Global Biogeochem. Cy., 20, GB2017, doi:10.1029/2005GB002591, 2006.
610 Aumont, O., Ethé, C., Tagliabue, A., Bopp, L., and Gehlen, M.: PISCES-v2: an ocean
611 biogeochemical model for carbon and ecosystem studies, Geosci. Model Dev., 8, 2465–
612 2513, https://doi.org/10.5194/gmd-8-2465-2015, 2015.
613 Behrenfeld, M. J. and Falkowski, P. G.: Photosynthetic rates derived from satellite-based
614 chlorophyll concentration, Limnol. Oceanogr., 42, 1–20, 1997.
615 Clement, A. C., R. Seager, and R. Murtugudde (2005), Why are there tropical warm pools?,
616 J. Clim., 18, 5294–5311.
617 CSIRO: Atlas of Regional Seas, available at: http://www.marine.
618 csiro.au/~dunn/cars2009/ (last access: 20 September 2021), 2009.
619 Doerffer, R. and Schiller, H: The MERIS Case 2 water algorithm, Int. J. Remote Sens., 28,
620 517–535, doi:10.1080/01431160600821127, 2007.
621 Egbert, G. D., and S. Y. Erofeeva (2002), Efficient inverse modeling of barotropic ocean
622 tides, J. Atmos. Ocean. Technol., 19(2), 183–204, doi:10.1175/1520-
623 0426(2002)019<0183:EIMOBO>2.0.CO;2.
624 Eppley, R. W. and Peterson, B. J.: Particulate organic matter flux and planktonic new
625 production in the deep ocean, Nature, 282, 677–680, 1979.
626 Ffield, A., and A. L. Gordon (1992), Vertical Mixing in the Indonesian Thermocline, J. Phys.
627 Oceanogr., 22(2), 184–195, doi:10.1175/1520-0485(1992)022<0184:VMITIT> 2.0.CO;2.
628 Ffield, A., and A. L. Gordon (1996), Tidal Mixing Signatures in the Indonesian Seas, J. Phys.
629 Oceanogr., 26(9), 1924–1937, doi:10.1175/15200485(1996)026<1924:TMSITI>
630 2.0.CO;2.
631 Ffield, A., and R. Robertson (2008), Temperature and finestructure in the Indonesian
632 Seas, J. Geophys. Res., 113, C09009, doi:10.1029/2006JC003864.

633 Fieux, M., Andrié, C., Delecluse, P., Ilahude, A.G., Kartavtseff, A., Mantisi, F., Molcard, R.,
634 Swallow, J.C., (1994), Measurements within the Pacific-Indian oceans throughflow
635 region. Deep. Res. Part I 41 (7), 1091–1130. http://dx.doi.org/10.1016/0967-
636 0637(94)90020-5.
637 Garcia, H. E., K. Weathers, C. R. Paver, I. Smolyar, T. P. Boyer, R. A. Locarnini, M. M.
638 Zweng, A. V. Mishonov, O. K. Baranova, D. Seidov, and J. R. Reagan, 2018a. World
639 Ocean Atlas 2018, Volume 3: Dissolved Oxygen, Apparent Oxygen Utilization, and
640 Oxygen Saturation. A. Mishonov Technical Ed.; NOAA Atlas NESDIS 83, 38pp.
641 Garcia, H. E., K. Weathers, C. R. Paver, I. Smolyar, T. P. Boyer, R. A. Locarnini, M.
642 M. Zweng, A. V. Mishonov, O. K. Baranova, D. Seidov, and J. R. Reagan, 2018b.
643 World Ocean Atlas 2018, Volume 4: Dissolved Inorganic Nutrients (phosphate, nitrate
644 and nitrate+nitrite, silicate). A. Mishonov Technical Ed.; NOAA Atlas NESDIS 84, 35p
645 Geider, R. J., MacIntyre, H. L., and Kana, T. M.: A dynamic model of phytoplankton growth
646 and acclimation: responses of the balanced growth and Chlorophyll a : carbon ratio to
647 light, nutrient-limitation and temperature, Mar. Ecol.-Prog. Ser., 148, 187–200, 199
648 Gordon, A. L: Oceanography of the Indonesian seas and their throughflow, Oceanography,
649 18, 14–27, doi:10.5670/oceanog.2005.01, 2005.
650 Gordon, A. L., and R. A. Fine (1996), Pathways of water between the Pacific and Indian
651 oceans in the Indonesian seas, Nature, 379(6561), 146–149.
652 Gutknecht, E., G. Reffray, M. Gehlen, I. Triyulianti, D. Berlianty, and P. Gaspar, (2016),
653 Evaluation of an operational ocean model configuration at 1/12° spatial resolution for the
654 Indonesian seas (NEMO2.3/INDO12) – Part 2: Biogeochemistry Geosci. Model Dev., 9,
655 1523–1543, www.geosci-model-dev.net/9/1523/2016/ doi:10.5194/gmd-9-1523-2016.
656 Hautala, S. L., J. Sprintall, J. T. Potemra, J. C. Chong, W. Pandoe, N. Bray, and a. G.
657 Ilahude, (2001), Velocity structure and transport of the Indonesian throughflow in the
658 major straits restricting flow into the Indian Ocean, J. Geophys. Res., 106(C9), 19527,
659 doi:http://dx.doi.org/10.1029/2000JC000577.
660 Holloway, G., and K. Denman (1989), Influence of internal waves on primary production, J.
661 Plankton Res., 11(2), 409–413.
662 Jochum, Markus ; Potemra, J. (2008), Sensitivity of Tropical Rainfall to Banda Sea
663 Diffusivity in the Community Climate System Model. In: Journal of Climate. 2008 ; Vol.
664 21. pp. 6445-6454.
665 Kida, S., and S. Wijffels (2012), The impact of the Indonesian Throughflow and tidal mixing
666 on the summertime sea surface temperature in the western Indonesian Seas, J. Geophys.
667 Res. Ocean., 117(9), 1–14, doi:10.1029/2012JC008162.
668 Kinkade, C.S., Marra, J., Dickey, T., Langdon, C., Sigurdson, D.E., Weller, .R., 1999. Diel
669 bio-optical variability observed from moored sensors in the Arabian Sea. Deep-Sea
670 Research Part II 46, 1813}1832.
671 Koch-Larrouy, A., G. Madec, D. Iudicone, A. Atmadipoera, and R. Molcard (2008), Physical
672 processes contributing to the water mass transformation of the Indonesian Throughflow,
673 Ocean Dyn., 58, 275–288.
674 Koch-Larrouy, A., A. Atmadipoera, P. van Beek, G. Madec, J. Aucan, F. Lyard, J. Grelet,
675 and M. Souhaut (2015), Estimates of tidal mixing in the Indonesian archipelago from
676 multidisciplinary INDOMIX in-situ data, Deep. Res. Part I Oceanogr. Res. Pap., 106,
677 136–153, doi:10.1016/j.dsr.2015.09.007.

678 Koch-Larrouy, A., G. Madec, P. Bouruet-Aubertot, T. Gerkema, L. Bessières, and R.
679 Molcard (2007), On the transformation of Pacific Water into Indonesian Throughflow
680 Water by internal tidal mixing, Geophys. Res. Lett., 34(4), 1–6,
681 doi:10.1029/2006GL028405.
682 Koch-Larrouy, A., M. Lengaigne, P. Terray, G. Madec, and S. Masson (2010), Tidal mixing
683 in the Indonesian seas and its effect on the tropical climate system, Clim. Dyn.,
684 34(6), 891–904, doi:10.1007/s00382-009-0642-4.
685 Koch-Larrouy, A., Morrow, R., Penduff, T., and Juza, M., (2010), Origin and mechanism of
686 Subantarctic Mode Water formation and trans- formation in the Southern Indian Ocean,
687 Ocean Dynam., 60, 563–583, doi:10.1007/s10236-010-0276-4.
688 Koropitan, A. F. and M. Ikeda, (2016), Influences of physical processes and anthropogenic
689 influx on biogeochemical cycle in the Java Sea numerical model experiment, Procedia
690 Environmental Sciences 33, 532 – 552 doi:10.1016/j.proenv.2016.03.106.
691 Lellouche, J.-M., Le Galloudec, O., Drévillon, M., Régnier, C., Greiner, E., Garric, G., Ferry,
692 N., Desportes, C., Testut, C.-E., Bricaud, C., Bourdallé-Badie, R., Tranchant, B.,
693 Benkiran, M., Drillet, Y., Daudin, A., and De Nicola, C., (2013): Evaluation of global
694 monitoring and forecasting systems at Mercator Océan, Ocean Sci., 9, 57–81,
695 doi:10.5194/os-9-57-2013
696 Madec, G. (2008), NEMO ocean engine, Note du Pole de modélisation, Institut Pierre-Simon
697 Laplace (IPSL), France, No. 27, ISSN No. 1288–1619.
698 Madec, G., Delecluse, P., Imbard, M., and Lévy, C.: “OPA 8.1 Ocean General Circulation
699 Model reference manual”, Note du Pole de modélisation, Institut Pierre-Simon Laplace
700 (IPSL), France, No. 11, 91 pp., 1998.
701 Maraldi, C., Chanut, J., Levier, B., Ayoub, N., De Mey, P., Reffray, G., Lyard, F., Cailleau,
702 S., Drévillon, M., Fanjul, E. A., Sotillo, M. G., Marsaleix, P., and the Mercator Research
703 and Development Team (2013), NEMO on the shelf: assessment of the Iberia–Biscay–
704 Ireland configuration, Ocean Sci., 9, 745-771, doi:10.5194/os-9-745-2013.
705 Meyers, G., (1996), Variation of Indonesian throughflow and the El Niño-Southern
706 Oscillation, J. Geophys. Res., 101, 12475–12482.
707 Molcard, R., Fieux, M., Syamsudin, F., (2001), The throughflow within Ombai Strait. Deep.
708 Res. Part I Oceanogr. Res. Pap. 48 (5), 1237–1253. http://dx.doi.org/10.1016/S0967-
709 0637(00)00084-4.
710 Mora, C., P. M. Chittaro, P. F. Sale, J. P. Kritzer, S. a. Ludsin, and S. Africa, (2003), Patterns
711 and processes in reef fish diversity, Nature, 421(February), 933–936,
712 doi:10.1038/nature01421.1.
713 Murray, S.P., Arief, D., (1988). Throughflow into the Indian Ocean through the
714 LombokStrait, January 1985–January 1986. Nature 333 (6172), 444–447.
715 http://dx.doi.org/10.1038/333444a0.
716 Nagai, T., and T. Hibiya (2015), Internal tides and associated vertical mixing in the
717 Indonesian Archipelago, J. Geophys. Res. C Ocean., 3373–3390,
718 doi:10.1002/2014JC010592.
719 Nagai, T., Hibiya, T., & Bouruet- Aubertot, P. (2017). Nonhydrostatic simulations of tide-
720 induced mixing in the Halmahera Sea: A possible role in the transformation of the
721 Indonesian Throughflow waters. Journal of Geophysical Research: Oceans, 122,8933–
722 8943. https://doi.org/10.1002/2017JC013381.

723 Nagai, T., Hibiya, T., & Syamsudin, F. (2021). Direct estimates of turbulent mixing in the
724 Indonesian archipelago and its role in the transformation of the Indonesian throughflow
725 waters. Geophysical Research Letters, 48, e2020GL091731.
726 https://doi.org/10.1029/2020GL091731.
727 Neale, R., & Slingo, J. (2003). The Maritime Continent and Its Role in the Global Climate: A
728 GCM Study, *Journal of Climate*, *16*(5), 834-848. Retrieved Jul 4, 2022, from
729 https://journals.ametsoc.org/view/journals/clim/16/5/1520-
730 0442_2003_016_0834_tmcair_2.0.co_2.xm.
731 Niwa, Y., and T. Hibiya (2011), Estimation of Internal Tide Energy Available for
732 Deep Ocean Mixing Based on Three-dimensional Global Numerical Simulations
733 Energy Diagram for the Thermohaline Circulation ´The Mixing Energy Previous
734 Estimates of Global Energy Conversion Rate From the Sur, North, 1–15,
735 doi:10.1007/s10872-011- 0052-1
736 Nugroho, Koch-Larouy, Gaspar, Lyard et al. 2018, Modelling Explicit tides in the
737 Indonesian seas: an important process for surface sea water properties, Marine
738 Pollution Bulletin, http://dx.doi.org/10.1016/j.marpolbul.2017.06.033
739 Ray, R. D., and R. D. Susanto (2016), Tidal mixing signatures in the Indonesian seas
740 from high-resolution sea surface temperature data, Geophys. Res. Lett., 43(15),
741 8115– 8123, doi:10.1002/2016GL069485.
742 Rixen, T., Ittekkot, V., Herunadi, B., Wetzel, P., Maier Reimer, E., and Gaye-Haake,
743 B.: ENSO-driven carbon see saw in the Indo-Pacific, Geophys. Res. Lett., 33,
744 L07606, doi:10.1029/2005GL024965, 2006.
745 Shi, W., M. Wang, and L. Jiang (2011), Spring-neap tidal effects on satellite ocean
746 color observations in the Bohai Sea, Yellow Sea, and East China Sea, J.
747 Geophys. Res., 116, C12032, doi:10.1029/2011JC007234.
748 Shriver, J. F., B. K. Arbic, J. G. Richman, R. D. Ray, E. J. Metzger, A. J. Wallcraft,
749 and P. G. Timko (2012), An evaluation of the barotropic and internal tides in a high-
750 resolution global ocean circulation model, J. Geophys. Res., 117,C10024,
751 doi:10.1029/2012JC008170.
752 Simon B. (2013). Coastal Tides. Translated by David Manley; Monaco: Institut
753 Oceanographique, Paris, 409pp.
754 Song, Q., and A. Gordon. 2004. Significance of the vertical profile of Indonesian
755 throughflow transport on the Indian Ocean. Geophysical Research Letters
756 31:L16307, doi:10.1029/ 2004GL020360.
757 Souza, A. J., and J. Pineda (2001), Tidal mixing modulation of sea-surface
758 temperature and diatom abundance in Southern California, Cont. Shelf Res., 21(6–
759 7), 651–666, doi:10.1016/S0278-4343(00)00105-9.
760 Sprintall, J., S. E. Wijffels, R. Molcard, and I. Jaya (2009), Direct estimates of the
761 Indonesian Throughflow entering theIndian Ocean: 2004 – 2006,J. Geophys.
762 Res.,114, C07001, doi:10.1029/2008JC005257.
763 Sprintall, J., A. L. Gordon, A. Koch-Larrouy, T. Lee, J. T. Potemra, K. Pujiana, S. E.
764 Wijffels, and S. E. Wij (2014), The Indonesian seas and their role in the
765 coupled ocean–climate system, Nat. Geosci., 7(7), 487–492,
766 doi:10.1038/ngeo2188.
767 Sprintall, J., A. L. Gordon, S. E. Wijffels, M. Feng, S. Hu, A. Koch-Larrouy, H.
768 Phillips, D. Nugroho, A. Napitu, K. Pujiana, R. D. Susanto, B. Sloyan, D.

769 Yuan, N. F. Riama, S. Siswanto, A. Kuswardani, Z. Arifin, A. J. Wahyudi, H.
770 Zhou, T. Nagai, J. K. Ansong, R. Bourdalle-Badié, J. Chanut, F. Lyard, B. K.
771 Arbic, A. Ramdhani, A. Setiawan, Detecting Change in the Indonesian Seas, Front.
772 Mar. Sci., 04 June 2019, doi.org/10.3389/fmars.2019.00257.
773 Susanto, R. D., and A. L. Gordon (2005), Velocity and transport of the Makassar
774 Strait throughflow, J. Geophys. Res., 110, C01005, doi:10.1029/2004JC002425.
775 Susanto, R. D. and Marra, J., (2005), Effect of the 1997/98 El Niño on chlorophyll a
776 variability along the southern coasts of Java and Sumatra, Oceanography, 18,
777 124–127, doi:10.5670/oceanog.2005.13.
778 Susanto, R. D., Gordon, A. L., and Zheng, Q., (2001), Upwelling along the coasts of
779 Java and Sumatra and its relation to ENSO, Geophys. Res. Lett., 28, 1599–1602,
780 doi:10.1029/2000GL011844.
781 Susanto, R. D., Moore, T. S., and Marra, J.: Ocean color variability in the Indonesian
782 Seas during the SeaWiFS era, Geochemistry Geophysics Geosystems, 7,
783 Q05021, doi:10.1029/2005GC001009, 2006.
784 Tranchant, B., G. Reffray, E. Greiner, D. Nugroho, A. Koch-Larrouy, and P. Gaspar
785 (2016), Evaluation of an operational ocean model configuration at 1/12 spatial
786 resolution for the Indonesian seas . Part I : ocean physics, 1–49, doi:10.5194/gmdd-8-
787 6669-2015.
788 Veron, J. E. N., L. M. Devantier, E. Turak, A. L. Green, S. Kininmonth, M.
789 Stafford- Smith, and N. Peterson (2009), Delineating the Coral Triangle, Galaxea, J.
790 Coral Reef Stud., 11(2), 91–100, doi:10.3755/galaxea.11.91.
791 World Ocean Atlas, (2018), available at:
792 https://www.nodc.noaa.gov/cgi-bin/OC5/woa18/woa18.pl (last access: 20
793 September 2021).
794 Xing Q, Yu H, Yu H, Wang H, Ito S-i and Yuan C (2021) Evaluating the Spring-
795 Neap Tidal Effects on Chlorophyll-a Variations Based on the Geostationary
796 Satellite. Front. Mar. Sci. 8:758538. doi: 10.3389/fmars.2021.758538.
797 Zaron E. D. (2018), Ocean and ice shelf tides from CryoSat-2 altimetry. *J. Phys.*
798 *Oceanogr.*, 48:975–993.
799 Zaron E. D., Capuano T. A., Koch-Larrouy A. (2022), Tidal Variability of Chl-a
800 in the Indonesian Seas. Submitted to Ocean Sciences Discussion.